Physics of Plasmas

Optical probing of relativistic plasma singularities

Cite as: Phys. Plasmas **27**, 052103 (2020); https://doi.org/10.1063/5.0004525
Submitted: 12 February 2020 • Accepted: 22 April 2020 • Published Online: 08 May 2020

Timur Zh. Esirkepov, Jie Mu, Yanjun Gu, et al.

View Online Export Citation CrossMark

ARTICLES YOU MAY BE INTERESTED IN

Relativistic plasma physics in supercritical fields
Physics of Plasmas **27**, 050601 (2020); https://doi.org/10.1063/1.5144449

Recoil effects on reflection from relativistic mirrors in laser plasmas
Physics of Plasmas **27**, 032109 (2020); https://doi.org/10.1063/1.5142084

Perspectives on the generation of electron beams from plasma-based accelerators and their near and long term applications
Physics of Plasmas **27**, 070602 (2020); https://doi.org/10.1063/5.0004039

AIP Publishing Physics of Plasmas Features in Plasma Physics Webinars Register Today!

AIP Publishing

© 2020 Author(s).

Physics of Plasmas ARTICLE scitation.org/journal/php

Optical probing of relativistic plasma singularities

Cite as: Phys. Plasmas **27**, 052103 (2020); doi: 10.1063/5.0004525
Submitted: 12 February 2020 · Accepted: 22 April 2020 ·
Published Online: 8 May 2020

Timur Zh. Esirkepov,[1,a)] Jie Mu,[2] Yanjun Gu,[2] Tae Moon Jeong,[2] Petr Valenta,[2] Ondrej Klimo,[2] James K. Koga,[1] Masaki Kando,[1] David Neely,[3,4] Georg Korn,[2] Sergei V. Bulanov,[1,2] and Alexander S. Pirozhkov[1]

AFFILIATIONS

[1]Kansai Photon Science Institute, National Institutes for Quantum and Radiological Science and Technology, 8-1-7 Umemidai, Kizugawa-city, Kyoto 619-0215, Japan
[2]Institute of Physics of the Czech Academy of Sciences, Extreme Light Infrastructure Beamlines Project, Na Slovance 2, 18221 Prague, Czech Republic
[3]Central Laser Facility, Rutherford Appleton Laboratory, Science and Technology Facilities Council, Chilton, Didcot, Oxon OX11 0QX, United Kingdom
[4]Department of Physics, Scottish Universities Physics Alliance, University of Strathclyde, Glasgow G4 0NG, United Kingdom

[a)]**Author to whom correspondence should be addressed:** timur.esirkepov@qst.go.jp

ABSTRACT

Singularities in multi-stream flows of relativistic plasmas can efficiently produce coherent high-frequency radiation, as exemplified in the concepts of the Relativistic Flying Mirror [Bulanov *et al.*, Phys. Rev. Lett. **91**, 085001 (2003)] and Burst Intensification by Singularity Emitting Radiation [Pirozhkov *et al.*, Sci. Rep. **7**, 17968 (2017)]. Direct observation of these singularities is challenging due to their extreme sharpness (tens of nanometers), relativistic velocity, and transient non-local nature. We propose to use an ultrafast (a few light cycles) optical probe for identifying relativistic plasma singularities. Our estimations and Particle-in-Cell simulations show that this diagnostic is feasible.

© 2020 Author(s). All article content, except where otherwise noted, is licensed under a Creative Commons Attribution (CC BY) license (http://creativecommons.org/licenses/by/4.0/). https://doi.org/10.1063/5.0004525

I. INTRODUCTION

Singularities easily form in multi-stream flows; they appear as crests or surges with respect to some physical parameters, which are usually continuous, e.g., density, pressure, etc. If these crests and surges correspond to structurally stable singularities, they are inevitable and robust with respect to modulations, as explained by catastrophe theory.[1,2] In relativistic underdense plasmas driven by intense femtosecond lasers, two particularly interesting examples of the cusp singularities appear in electron density: one in a breaking wake wave[3] and another at the joining of the cavity wall and the bow wave.[4,5]

In order to create these singularities, the driving laser should be sufficiently intense, with the dimensionless amplitude of the order of 1 or greater, $a_0 = eE_0/m_e c\omega_0 = (I_0/I_R)^{1/2} \geq 1$, and short, with the length comparable to or shorter than the Langmuir wavelength, $\tau_L \leq 2\pi/\omega_{pe}$. Here, c is the speed of light in vacuum; τ_L is the pulse duration; E_0, I_0, $\omega_0 = 2\pi c/\lambda_0$ and λ_0 are the laser electric field, irradiance, angular frequency, and wavelength, respectively; e and m_e are the electron charge and mass, respectively; $I_R = \pi c^5 m_e^2/2e^2\lambda_0^2 \approx 1.37 \times 10^{18}$ W/cm^2 $\times (\lambda_0[\mu\text{m}])^{-2}$ for a linearly polarized field; $\lambda_0[\mu\text{m}]$ denotes the wavelength in micrometers. We consider underdense plasma, with the initial electron density much less than the critical density, $n_e \ll n_{cr}$, where $n_{cr} = m_e\omega_0^2/4\pi e^2 \approx 1.1 \times 10^{21}$ cm$^{-3}(\lambda_0[\mu\text{m}])^{-2}$. This is equivalent to $\omega_{pe} \ll \omega_0$, where $\omega_{pe} = (4\pi e^2 n_e/m_e)^{1/2}$ is the Langmuir frequency. Under these conditions, the electron dynamics is relativistic; thus, the laser–plasma interaction is highly nonlinear. In particular, the Langmuir wave frequency nonlinearly depends on its amplitude.

The first above-mentioned cusp singularity appears when a wake wave, driven by a relativistically intense laser pulse, breaks. This happens, e.g., when the driver pulse is strong enough to accelerate electrons to a velocity exceeding the driver pulse group velocity,[6] $a_0 > (2\omega_0/\omega_{pe})^{2/3}$. Under optimum conditions, the cusp can take the form of a dense, thin shell moving behind the driving laser pulse with relativistic velocity. Due to the high density and sharpness, this shell can act as a Relativistic Flying Mirror, reflecting a counterpropagating laser pulse.[7–10] The frequency of the reflected light is upshifted and duration shortened due to the double Doppler effect, so that a high-frequency coherent pulse is produced; in addition, the shell can have a

© Author(s) 2020

concave, nearly parabolic, shape,[3,8] which focuses the reflected radiation to a tiny spot, promising record intensities beyond the capabilities of directly focused lasers.[8] The Relativistic Flying Mirror was demonstrated experimentally in Refs. 11–18, where the frequency upshift was sufficient to convert near infra-red laser radiation ($\lambda_0 \approx 0.8\,\mu$m) to coherent soft x-rays, down to $\lambda_x = 7$ nm.

The second mentioned cusp singularity appears when the bow wave detaches from the cavity wall, which happens when the laser spot is sufficiently narrow,[4] $d < d_{BW} = 2\lambda_0(a_0 n_{cr}/n_e)^{1/2}/\pi$. This can be achieved, for example, due to relativistic self-focusing,[19–21] where the spot size under stationary conditions can be estimated as[22] $d_0 = \lambda_0(a_0 n_{cr}/n_e)^{1/2}/\pi$ and the dimensionless amplitude as $a_0 = (8\pi P_0 n_e/P_c n_{cr})^{1/3}$, where the laser power P_0 exceeds the threshold $P_{SF} = P_c(n_{cr}/n_e)$ and[21] $P_c = 2m_e^2c^5/e^2 \approx 0.017$ TW. This cusp singularity is situated near the laser pulse head and is strongly driven by the laser field. The accelerated motion of the electrons in the singularity leads to high-frequency radiation, while the singularity sharpness ensures constructive interference, producing a bright coherent x-ray pulse[5,18,23–28] termed Burst Intensification by Singularity Emitting Radiation (BISER).[28] BISER has an unprecedentedly small source size: sub-μm measured directly (limited by the resolution of employed x-ray optics) and down to 10 nm predicted by the Particle-In-Cell (PIC) simulations.[28] Together with the attosecond duration (predicted by PIC) and large photon number (measured 10^{10} photons with energy from 60 to 100 eV), this gives a peak spectral brightness of up to 10^{27} photons/mm$^2\cdot$ mrad$^2\cdot$ s in a 0.1% bandwidth (BW), which is one of the brightest among laser-based sources.

The term "singularity" comes from a well-established model and fits well for the description of the electron density spikes seen in the laser–matter interactions. In a converging multi-stream flow, the density or its derivative increases due to stagnation of matter. This can happen not only with the density, but any other additive characteristic of the medium. In the approximation of continuous collisionless fluid, the density may become infinite, while its integral is still finite. This singularity appears in the projection of the complete phase space of the fluid onto a configuration space; such a situation is described by the catastrophe theory.[1,2] Among different possible singularities, there are structurally stable ones, such as folds and cusps. We identify folds as bow wave outlines and the boundaries of the electron cavity. The cusps correspond to electron density spikes at the joint of the cavity boundary with the bow wave outline. When the medium consists of discrete particles, density is not infinite. However, the larger the number of particles, the closer is the density of a stable spike to the theoretically predicted structurally stable singularity [see Fig. 5(d) in Ref. 5]. Therefore, there is an undeniable relation between the entities seen in simulations (density spikes) and the well-established model (singularities of multi-stream flows). The situation is analogous to the naming of a sinusoidal wave: observers cannot verify a true sinusoid in any physical phenomenon, simply because the corresponding mathematical function has infinite support and is infinitely differentiable. Nevertheless, in many cases, the relation between idealized models and physical phenomena allows us to use names of model entities for physical entities not only without serious contradiction, but with essential predictive power.

Direct experimental observation of these singularities is challenging due to their small size, relativistic velocity, and transient non-local nature. Here, we propose to use an ultrashort-duration (few-cycle) optical probe to detect these singularities using Schlieren imaging. In order to demonstrate the diagnostic feasibility, we specify the necessary probe pulse parameters, present relevant estimates, and show the results of PIC simulations.

A visualization of wake waves excited by intense laser pulses in underdense plasma recently became available with a new generation of laboratory diagnostics.[29–33] The use of ultrashort optical probe pulses for shadography of fast-moving wake waves has been demonstrated in Refs. 31–33. As the next step to these shadowgraphic measurements, the proposed Schlieren method removes the unperturbed part of the probe pulse. This emphasizes the spherical waves originating from the singularities and reduces the effect of the driver pulse on the probe phase.

Our simulations show that the probe pulse undergoes strong diffraction on the moving singularities producing spherical waves whose frequency depends on angle due to the relativistic effects. The corresponding upshifts or downshift of the probe frequency can be reliably detected at angles viewable with Schlieren imaging. We also show that our method reveals a phenomenon similar to the Lampa–Penrose–Terrell effect.[34]

II. SCHLIEREN IMAGING SCHEME

A possible experimental setup is shown in Fig. 1. An intense driver laser pulse with the dimensionless amplitude of $a_0 > 1$ is focused onto a supersonic gas jet. Since the magnitude of the driver

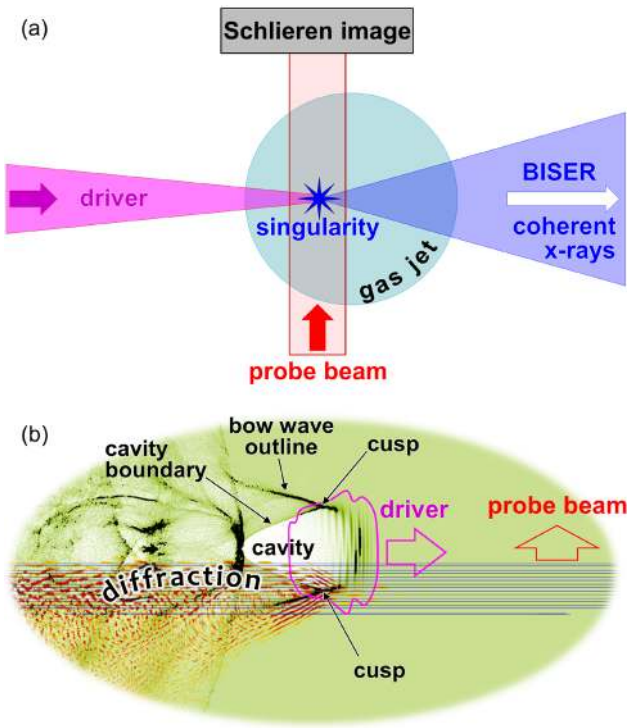

FIG. 1. (a) The proposed experimental setup. The driver laser pulse is focused onto a gas jet. The resulting BISER is detected in the direction of the driver. The singularities are imaged by the transverse probe ultrashort laser pulse. (b) Interaction of the driver and probe pulses with plasma with labeled physical entities of interest (the image is taken from PIC simulation).

© Author(s) 2020

field well exceeds that of the intra-atomic field, the gas becomes ionized with a time period shorter than the laser cycle. An underdense plasma is created. The driver pulse power is greater than the threshold of relativistic self-focusing. The self-focusing driver pulse excites a wake wave and bow wave, as seen below in the simulations. As described in Sec. I, the cusps formed near the driver pulse head emit coherent radiation, BISER.[28] It can be seen by an x-ray spectrometer placed within a relatively small angle about the direction of the driver pulse propagation.

A weak probe laser pulse is irradiated onto the plasma in the transverse direction, perpendicular to the driver pulse axis. It propagates through the channel created by the driver pulse, and then goes into a special optical system which makes a Schlieren image as shown in Fig. 2(a). The probe pulse is diffracted on singularities of electron density and electron current density, formed in the plasma by the driver pulse. These singularities are strongly localized; thus, they easily break the approximation of geometric optics. A singularity produces a spherical diffracted wave, Fig. 2(a), which is imaged by the lens as a point-like object. In this way, the singularities can be identified using Schlieren imaging. We note that the probe pulse length must be shorter than the longitudinal and transverse distances between the singularities, $c\tau < d_0$; otherwise, the spherical waves appear with their centers significantly drifting with time, so that different singularities become indistinguishable due to the longitudinal and transverse motion blurs.

We can roughly estimate the cusp singularity effect on the probe pulse phase by assuming a stationary cusp density distribution[5]

$$n_e(y) = n_0\left(\frac{\lambda}{y}\right)^{2/3}, \tag{1}$$

Fig. 2(b). The phase shift is

$$\Delta\phi = \frac{2\pi}{\lambda}\int(\mathfrak{n}-1)dy, \tag{2}$$

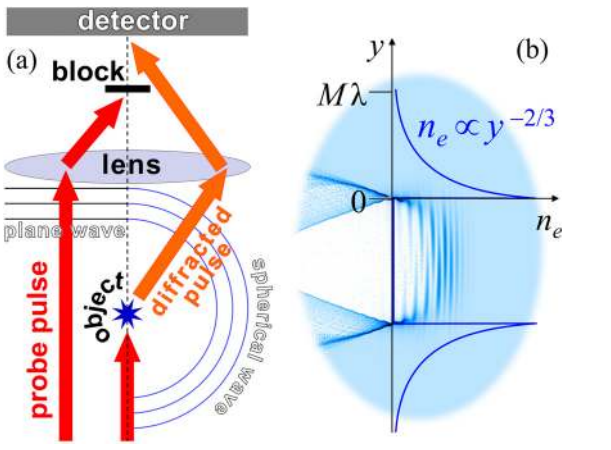

FIG. 2. (a) The principal scheme of the Schlieren imaging. The left half: the rays and wave fronts of the probe pulse; after transmission through the lens, the probe pulse is blocked by an opaque filter. The right half: the rays and wave fronts of the probe pulse diffracted at a point object; after transmission through the lens, the diffracted pulse is focused onto the detector, forming the image of the object. The actual configuration has rotational symmetry with respect to the axis denoted by the dashed line. (b) The scheme for the refractive index integration (see the text).

where $\mathfrak{n}$ is the refractive index

$$\mathfrak{n} = \sqrt{1 - n_e/n_{cr}}. \tag{3}$$

λ is the probe wavelength and y is the coordinate along the probe pulse propagation direction. The integration from 0 to $y_{\max} = M\lambda$, where M is the dimensionless length, gives the real part

$$\mathrm{Re}[\Delta\phi] = 2\pi\left((M^{2/3} - n_0/n_{cr})^{3/2} - M\right), \tag{4}$$

which slowly diverges as $\mathrm{Re}[\Delta\phi] \to -3\pi M^{1/3} n_0/n_{cr}$ at large M. We note that in 3D the electron density starts to decrease quickly at $y > d_0$, so for estimation, we can use $M = d_0/\lambda$. The imaginary part is

$$\mathrm{Im}[\Delta\phi] = 2\pi(n_0/n_{cr})^{3/2}, \tag{5}$$

corresponding to the transmission intensity of $\exp(-2\pi(n_0/n_{cr})^{3/2})$. For the cusp parameters as in Ref. 28 ($n_0 = 0.023 n_{cr}$), this gives the real part of $\mathrm{Re}[\Delta\phi] = -0.46$ rad and the imaginary part of $\mathrm{Im}[\Delta\phi] = 0.02$ rad, corresponding to the beam transmission of 0.96, i.e., 4% attenuation. Such a phase shift and attenuation are well within measurable ranges.

III. SIMULATION SETUP

It is sufficient to illustrate the possibility of Schlieren imaging in two-dimensional (2D) geometry. If diffraction is seen in 2D, it certainly exists also in 3D geometry. Previous experiments demonstrate that density cusps emit soft x-rays as point-like sources (see Ref. 28 for the case of a linearly polarized driver). As is well known, diffraction on objects, which are smaller than the incident wavelength, produces spherical wavefronts. The estimations in Sec. II confirm that the distortions of the probe pulse due to density cusps are detectable. Here, we use 2D PIC simulations performed with the REMP code[35] to demonstrate spherical wavefronts from the density cusps and the expected change of the frequency of the diffracted radiation due to the cusp fast motion.

The setup is shown in Fig. 3. The driver laser pulse with the wavelength of λ_0 propagates in the direction of the x-axis (in Figs. 3, 4, 6—from the left to the right). It is p-polarized, i.e., the electric field vector of its fundamental mode is in the direction of y-axis, in the plane of the simulation box. Initially, its electromagnetic field is given by E_x, E_y, B_z components while other components are zero. The driver pulse has a Gaussian shape with the full width at half maximum (FWHM) length of $5\lambda_0$ and the focal spot size of $5\lambda_0$. The driver amplitude is $a_0 = 6.6$; it is assumed that the focal plane is inside the plasma at the distance of $40\lambda_0$ from the vacuum–plasma interface, where the driver enters the plasma ("assumed," because the value is given for the case

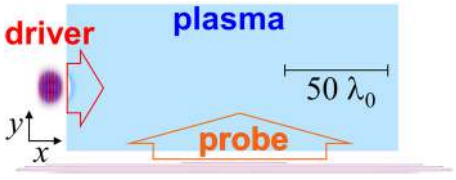

FIG. 3. The PIC simulation setup.

© Author(s) 2020

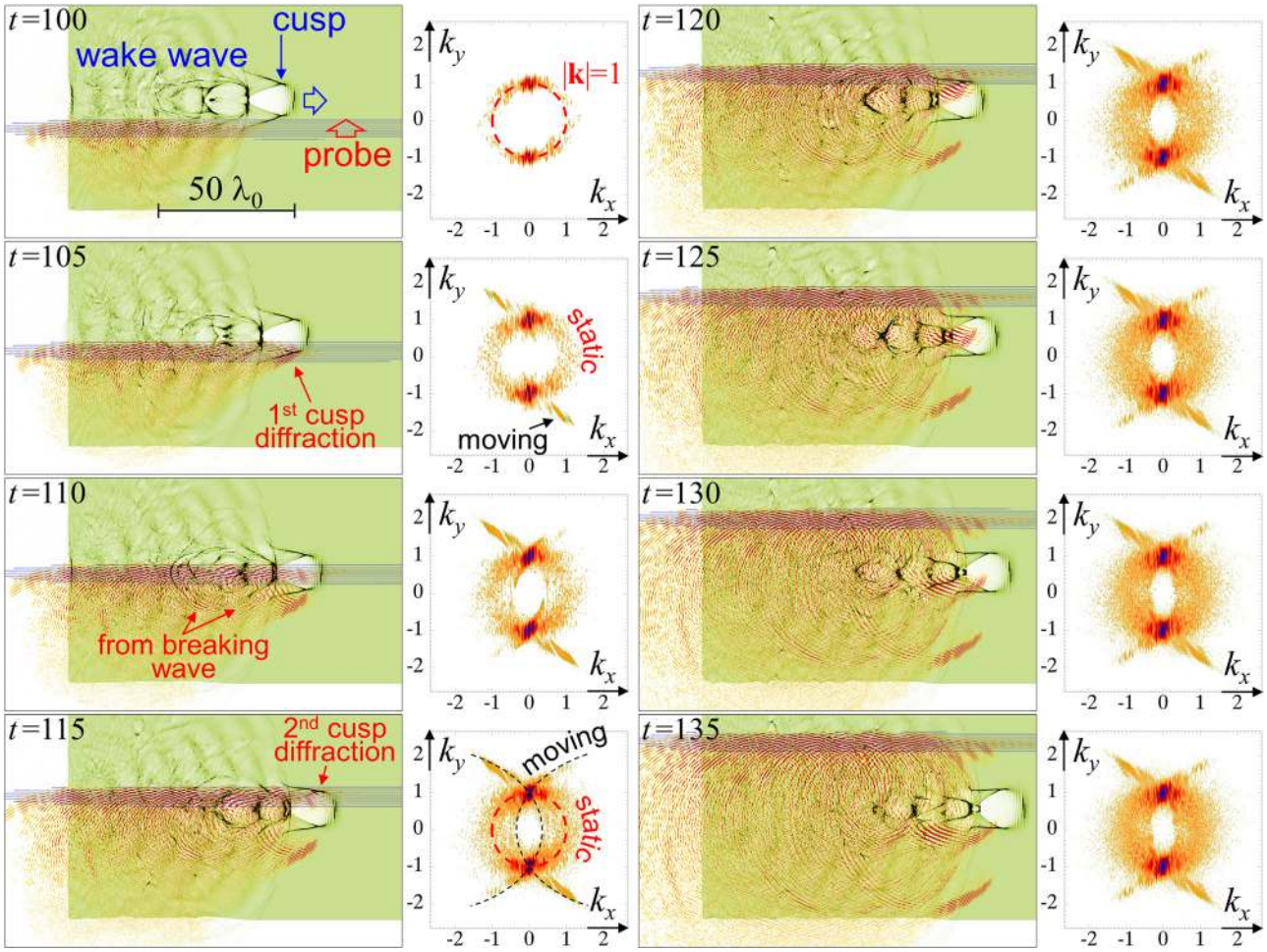

FIG. 4. The 1st and 3rd columns: the probe pulse propagation through the wake wave. Density modulations at the first wake wave cavity front reveal the driver laser pulse. The nearly horizontal curves for $E_z = 10^{-3}$ correspond to the bulk of the probe pulse. White-red colorscale for $0 < E_z^* < 5 \times 10^{-4}$ shows the difference between two simulations, one with the driver and probe and another with the probe only; the waves going in the vertical direction are filtered out (according to the Schlieren imaging) using a Fourier filter. Black curves for $n_e = 3n_{e0}$; white-green colorscale for $0 < n_e < 8n_{e0}$. The 2nd and 4th columns: the spatial spectrum of the E_z field component (not filtered). Wave vector is normalized by that of the probe pulse, k_0. The spectrum magnitude maxima at two darkest spots at $(k_x, k_y) = (0, \pm 1)$ correspond to the initial probe pulse direction and laser wavelength λ_0.

of the driver propagation in vacuum). The corresponding peak irradiance is 6×10^{19} W/cm^2 $\times$ $(\lambda_0\,[\mu\text{m}])^{-2}$, pulse power is 15 TW, and pulse energy is 240 mJ$\times(\lambda_0[\mu\text{m}])$.

The plasma slab is rectangular and has the sizes of $160\lambda_0$ and $80\lambda_0$ in the direction of the x and y axes, respectively. It is placed in the center of the simulation box with the size of $320\lambda_0 \times 320\lambda_0$. The initial electron density is $n_{e0} = 0.01 n_{cr} \approx 1.1 \times 10^{19}$ cm^{-3} $[\lambda_0\,(\mu\text{m})]^{-2}$.

The probe laser pulse, with the same wavelength as the driver pulse, $\lambda = \lambda_0$, propagates in the direction of the y-axis (in Figs. 3, 4, 6—from the bottom to the top). It is s-polarized, i.e., the electric field vector of its fundamental mode is in the direction of z-axis, perpendicular to the plane of the simulation box. The difference in the driver and probe polarization helps to distinguish the evolution of the driver and probe. As is well known, the interaction of a p-polarized electromagnetic wave with plasmas has a special symmetry in a 2D configuration: if only three components of the electromagnetic field, E_x, E_y, and B_z, and only two components of the plasma particles momentum, p_x and p_y, are initially non-zero, then all the other components will be zero forever. Thus, in the interaction of a p-polarized driver with an initially calm plasma, the components E_z, B_x, and B_y can acquire non-zero values only in the presence of the s-polarized probe.

Different polarization of the probe pulse helps to filter out plasma emission due to the driver pulse. In the plane perpendicular to the driver pulse polarization, emission of electrons dragged by the driver is much less efficient; therefore, it makes much less impact on the imaging by the probe. We also note that the s-polarized probe is not sensitive to the driver magnetic field,[33] which simplifies the analysis.

The probe pulse also has a Gaussian shape with the FWHM length of $3\lambda_0$ and the focal spot size of $(160/3)\lambda_0$ (we note that in

© Author(s) 2020

Ref. 31, experiments were done with a probe pulse duration of 6 fs, which corresponds to ~2 laser cycles). Its amplitude is $a_0 = 0.01$; it is assumed that the focal plane is at the bottom plasma–vacuum interface (for such a wide probe pulse, its Rayleigh length is much greater than the transverse extent of the plasma slab). The probe pulse amplitude is small enough to prevent significant modification of the wake wave structure; in experiments, it can be a few orders of magnitude less. The probe is sent into the plasma 50 laser cycles later than the driver, so that the probe propagates through the wake wave when the driver is approximately at the center of the plasma slab. The mesh size is $\lambda_0/16$ in both spatial directions, which is sufficient to see slightly more than the second harmonic. The time step is 0.999 of the threshold corresponding to the Courant–Friedrichs–Lewy condition. The number of quasi-particles per cell is 1; the plasma consists of electrons with a neutralizing background of immobile ions.

IV. SIMULATION RESULTS

The results of simulations are presented in Figs. 4–6. In the figures, the time unit is the laser cycle, $T_0 = \lambda_0/c$. The driver and probe pulses enter the plasma approximately at $t = 20$ and $t = 70$, respectively.

In order to show a portion of the probe laser pulse, which is diffracted, we performed two different simulations: in one run both the driver and the probe pulses are present, in another run only the probe pulse is present. In both runs, the probe pulse is very weak, so it is possible to separate the resulting electromagnetic field into parts as follows. In the first run (with the driver and probe), the resulting E_{z1} component consists of the initial unperturbed probe pulse, E_{zp}; the probe pulse refracted by calm plasma, including reflection from plasma boundaries, E_{zpr}; and the radiation due to interaction of plasma with both the driver and probe, E_{zw}. Note that the driver itself cannot induce plasma emission with non-zero E_z in our configuration. As a result

$$E_{z1} = E_{zp} + E_{zpr} + E_{zw}. \tag{6}$$

In the second run (with the probe only), the resulting E_{z2} component consists only of the initial unperturbed probe pulse, E_{zp}, and the probe pulse refracted by calm plasma, including reflection from boundaries, E_{zpr}

$$E_{z2} = E_{zp} + E_{zpr}. \tag{7}$$

Thus, the difference between two runs consists only of the plasma emission due to both the driver and probe

$$E_z = E_{z1} - E_{z2} = E_{zw}. \tag{8}$$

This difference gives the desired diffraction from density singularities and any other possible radiation due to the interaction of the driver, probe, and plasma. As a beneficial side effect, this method allows removing refraction and reflection of the probe pulse at the plasma slab boundaries (undesirable for presentation).

In addition, the blocking technique in the Schlieren imaging is simulated by applying a Fourier filter, which removes modes propagating in the direction of the probe pulse

$$E_z^* = \mathscr{F}_{x,y}^{\mathrm{inv}}\left\{\mathscr{F}_{k_x,k_y}\{E_z(x,y)\}G(k_x,k_y)\right\}, \tag{9}$$

where the filter $G(k_x, k_y) = 0$ for $|k_x/k_0| < 0.156$ and everywhere else $G(k_x, k_y) = 1$. Here, $k_0 = 2\pi/\lambda_0$, $\mathscr{F}_{k_x,k_y}$, and $\mathscr{F}_{x,y}^{\mathrm{inv}}$ are the direct and inverse fast Fourier transform, respectively. The E_z^* component of the resulting field is shown in Figs. 4–6 by a white-red colorscale.

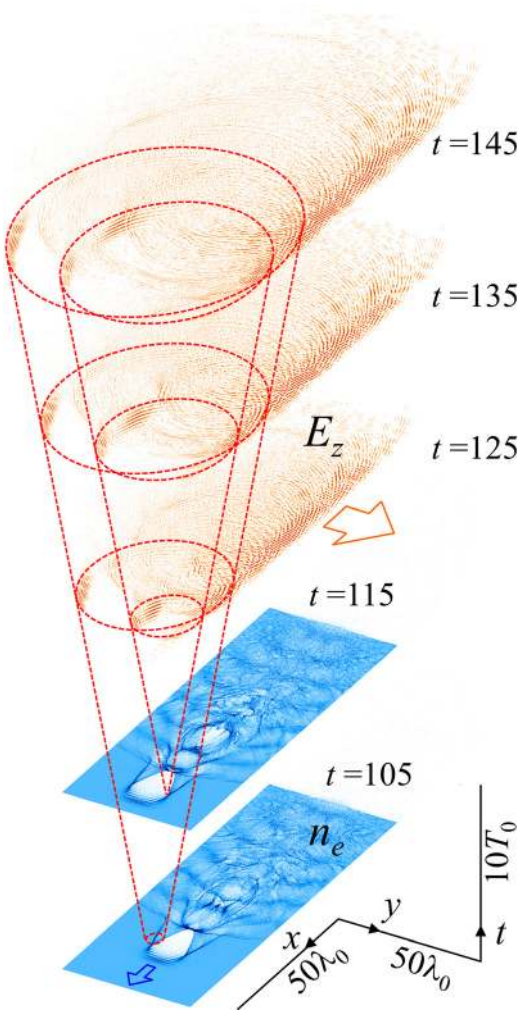

FIG. 5. A propagation of pulses created during the probe pulse diffraction on the plasma singularities. Frames with electron density (n_e, blue) and E_z^* field component (red) are placed along the time axis. The light cones represented by red dashed curves reveal the sources of the diffracted pulses.

The step described by Eq. (9) may seem superfluous, since E_z defined by Eq. (8) already removes refraction by calm plasma. However, the plasma channel created by the driver has a different refractive index and is asymetrically modulated. Thus, some portion of the probe pulse is refracted by the channel exactly in the vertical direction, but with different phase. This portion is undesirable because its magnitude is relatively high. The transformation of Eq. (9), corresponding to the blocking in the Schlieren imaging, removes this portion of the refracted probe beam.

Figure 4 shows the propagation of the probe laser pulse through plasma where the driver laser pulse excites plasma waves. The driver pulse can be traced by the electron density modulations with the laser wavelength at the front of the leading wake wave cavity. The laser

© Author(s) 2020

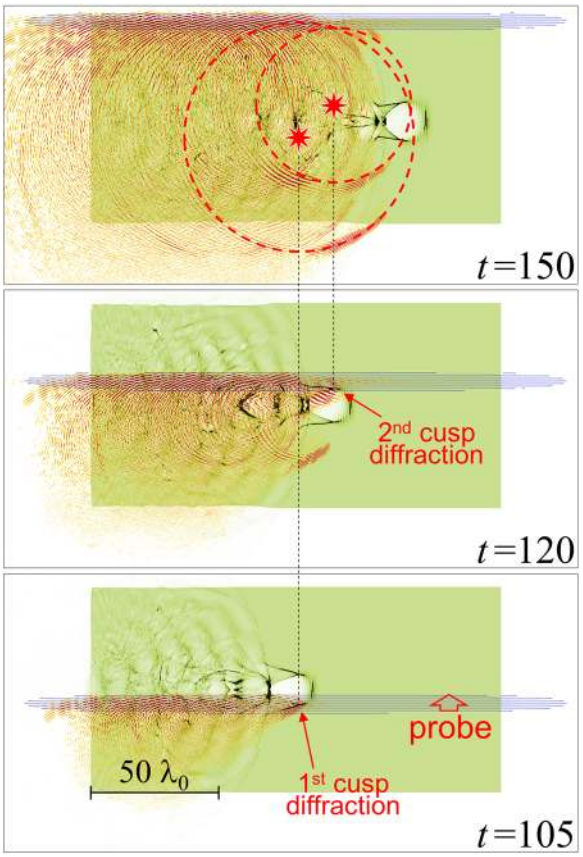

FIG. 6. Apparent rotation of a moving constellation of cusps. Colorscales and solid curves are the same as in Fig. 4. The 1st cusp at $t = 105$ and the 2nd cusp at $t = 120$ produce spherical fronts shown at $t = 150$ by thick dashed red circles. Each circle radius equals to the time period between the corresponding frames multiplied by the speed of light.

pulse is intense enough to accelerate electrons so that they cannot be bounded in the Langmuir oscillations. Therefore, the wake waves break. The resulting multi-stream flows of electrons form various density singularities seen as the low-dimensionality regions of high electron density. In particular, (one-dimensional) thin high-density shells (e.g., the cavity walls and the bow wave fronts) correspond to the fold singularity. The (zero-dimensional) points joining these thin shells correspond to the cusp singularity. We note that in a three-dimensional configuration, the mentioned examples of fold and cusp singularities are two- and one-dimensional, respectively,[4,5] and other types of singularities appear, e.g., the swallow tail singularity.[3]

The cusp singularity is produced near the front of the leading wake wave cavity due to a transverse wave-breaking; it is labeled at $t = 100$ in Fig. 4. The same type of singularity appears due to longitudinal wave-breaking at the ends of the 1st and 2nd wake wave periods. The characteristic size of the high electron density regions corresponding to the fold and cusp singularities is well below the driver laser wavelength. Thus, the electromagnetic emission from electrons in these regions, induced by the probe pulse, is coherent for wavelengths close to λ_0 (actually, even for much shorter wavelengths, of the order of the characteristic size of the high-density region[28]). Furthermore, these regions consist of electrons evacuated from the cavity. For the case of $\lambda_0 = 1\ \mu$m, we can roughly estimate the number of electrons from the cavity as $N_e = (4/3)\pi(10\lambda_0)^3 n_{e0} \approx 4.6 \times 10^{10}$. Taking into account the quadratic dependence of the coherent emission intensity on the number of emitters, it is not surprising that the probe pulse undergoes efficient diffraction on the density singularities.

A prominent diffraction occurs on the cusps at the head of the leading cavity at $t = 105$ and $t = 115$. The diffracted light appears in the form of short pulses with characteristic spherical wavefronts slightly shifted with respect to each other along the x-axis due to the cusp motion (a manifestation of the Doppler effect). The magnitude of this shift is determined by the velocities of the cusp and probe pulse, and by the duration of the probe pulse.

The spatial spectrum of the E_z field component defined in Eq. (8) and representing the plasma emission due to both the driver and probe reveals a characteristic angular distribution and its evolution, Fig. 4. The spectral maxima at the two darkest spots at $(k_x, k_y) = (0, \pm k_0)$ correspond to the initial probe pulse direction and laser wavelength λ_0. In Fig. 4, the wave-vector k components are normalized by k_0. The circle $k_x^2 + k_y^2 = k_0^2$ corresponds to waves with the wavelength of λ_0 going in all possible directions. This circle appears very early, $t \leq 100$, due to the diffraction of the probe pulse on quasi-static density modulations. We note that a significant portion of the electrons in the wake wave is not relativistic. These electrons have relatively small velocities, which leads to the corresponding broadening of the circle.

At $t = 105$, the characteristic "protrusions" emerge out of the circle into a higher frequency spectral domain. This emergence correlates with the onset of the probe pulse interaction with the 1st cusp. The protrusions correspond to the diffraction off moving objects. Therefore, due to the Doppler effect, they are arranged along an ellipse given by the formula (see Ref. 11)

$$\omega = c\sqrt{k_x^2 + k_y^2} = \frac{\omega_0}{1 - \beta\cos\alpha}, \tag{10}$$

$$\alpha = \arctan(k_y/k_x). \tag{11}$$

Here, β is the velocity of the cusp normalized by c. Equation (10) is essentially the famous Einstein formula for the frequency of light reflected from a relativistic mirror; it represents an ellipse in polar coordinates with angle α and radius ω, so that the leftmost focus of the ellipse is in the coordinates' origin. In the direction of the cusp motion, the diffracted wave frequency is upshifted; in the opposite direction, it is downshifted. We note that even though the frequency gets upshifted and downshifted in different directions, the diffracted wave fronts are always spherical, according to the special relativity theory.

The spectra reveal that the plasma emission due to simultaneous action of the driver and probe pulses consists of two distinct parts. One part is represented by frequencies arranged along an ellipse which correspond to the Einstein formula. It is labeled "moving." It is radiation diffracted from relativistically moving singularities. Another part is represented by frequencies arranged along a circle with radius $\omega_0 = ck_0$. It is labeled "static." It is radiation diffracted from a non-relativistic portion of the wake wave.

The diffraction on cusps embraces both transmission in the direction of the probe pulse and reflection in different directions. In Fig. 4, at $t = 105$ and subsequent moments in time, the spatial

© Author(s) 2020

distributions of the E_z^* component reveal strikingly efficient reflection off the bow wave related to the 1st cusp, similar to a specular reflection from a small flat mirror. This effect is described in detail in Ref. 36, for the case of a head-on collision with the probe pulse.

As seen in Fig. 4, during the propagation through the wake wave, the probe pulse becomes "enriched" with spherical wavefronts which originate at various singularities appearing in the wake wave. Figure 5 shows light cones formed by such spherical wavefronts emitted by two cusps at the head of the leading cavity, in Minkowski space (x, y, t). Different trains of spherical wavefronts with different curvature correspond to different strongly localized objects irradiated by the probe pulse at different times. These trains can be collected by a lens or other optical instruments which focus spherical wavefronts into diffraction-limited spots (in the idealized case). Using the Schlieren imaging scheme as in Fig. 2, one can obtain a snapshot of a moving constellation of electron density singularities, blurred due to a finite duration of the probe pulse. As is seen from the top parts of Figs. 5 and 6, the spherical wavefronts from both cusps are well discernible, although the wavefront from the cusp situated further from the detector can be distorted by the relativistic plasma channel and its image may be somewhat blurred.

The image of the constellation of singularities will be such as if the singularities were slightly rotated with respect to each other, Figs. 6 and 7. This phenomenon is similar to the Lampa–Penrose–Terrell effect.[34] The singularities move with the velocity approximately equal to the group velocity of the driver pulse, which is close to the speed of light in vacuum, c. The constellation of singularities significantly drifts during the probe pulse propagation through it. Therefore, parts of the constellation, which are irradiated later, appear in the image at positions more shifted in the direction of the constellation drift. This is seen in Fig. 6. If the cusps were at rest, the two spherical waves from them would have their centers exactly aligned along the probe pulse propagation, thus we would see just one diffracting object, Fig. 7(a). However, due to the fast motion of the cusps, the probe pulse meets them at different horizontal position. This results in the apparent rotation of the pair of cusps as a whole, so that we will see two separated diffracting objects, Figs. 6 and 7(b). For this, the probe pulse must be short enough, as stated above. In our case, the probe pulse is shorter than the constellation size, which is about the waist of the driver pulse along the y-axis. Figure 7(c) sketches out how the cusp is imaged in 3D geometry. The cusp singularity appears in the form of a ring.[4] Due to the linear polarization of the driver, more electrons concentrate in the direction of the driver polarization.[5,28] Since regions with higher electron density diffract light more efficiently, we see a sort of ellipse with a higher signal magnitude at two opposite spots.

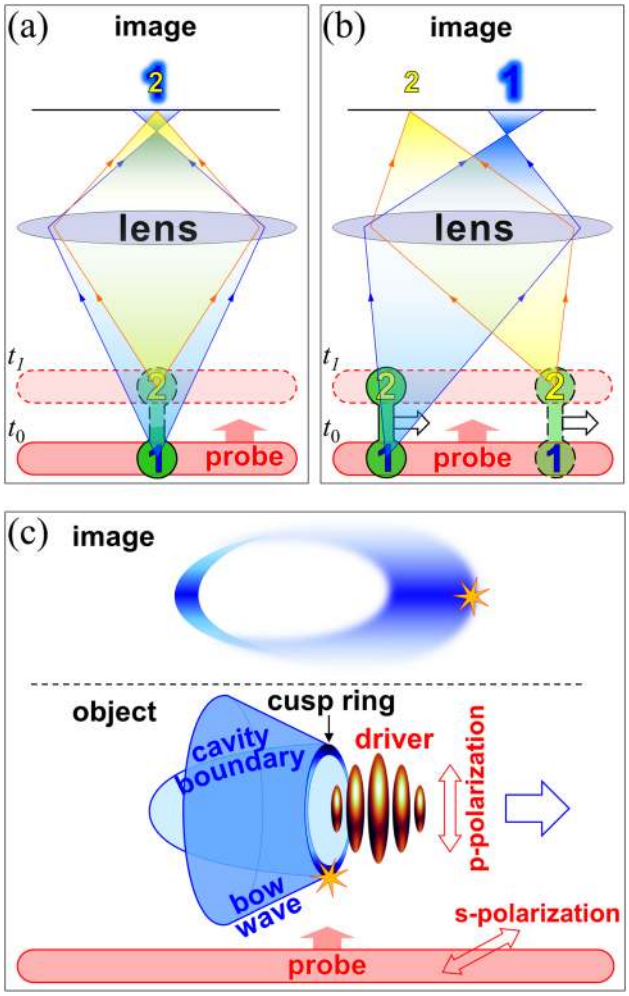

FIG. 7. The scheme of the observation of a static (a) and moving (b) elongated object through lens. A short probe laser pulse irradiates one end of the object at time t_0 and another end at time $t_1 > t_0$. (c) A sketch of an expected image of the cusp singularity in the experiment. The star shows which point of the object corresponds to which point in the image. As in the frames (a) and (b), the nearest to the detector point of the cusp ring is in the focus. It appears as the leftmost spot of the ellipse in the image.

V. CONCLUSION

Singularities are ubiquitous in relativistic plasma driven by an intense laser. They appear in multi-stream flows formed due to wave-breaking, which is a manifestation of a strongly nonlinear laser-plasma interaction. Electron density singularities in the wake of a relativistically strong laser pulse efficiently produce coherent x-ray radiation via several mechanisms such as BISER[5] and Relativistic Flying Mirror.[7,8]

In general, wave breaking causes electron injection into the accelerating phase of a strong Langmuir wave; in the course of wave breaking, the electron density exhibits a few types of singularities at the location of the injection; some of them are inevitably imprinted into the momentum and energy distribution of particles in the resulting accelerated electron bunch. Moreover, the acceleration of injected electrons in the Langmuir wave also produces characteristic fold singularity in the energy distribution of accelerated electrons.[37] Bunches of accelerated electrons in laser-driven plasma are often considered as sources of a bright x-ray radiation.[38–42] Since the emission efficiency strongly depends on the bunch parameters and characteristic motion in the wake wave, the presence of density singularities in the history of the bunch formation can strongly enhance the emission efficiency. Thus, singularities play an important role in the laser-driven electron injection and acceleration, as well as generation of high-frequency radiation, in particular, betatron radiation.

An ability to detect the singularities would be very advantageous for the experiments.[5,10–18,24–26,28–33,38–42] However, their direct

© Author(s) 2020

observation is challenging: as shown by simulations and experiments;[28] singularities have nano-scale dimensions and move with relativistic velocities. Using analytical estimates and 2D PIC simulations, we show that imaging of relativistically moving singularities in laser plasma is feasible using an ultra-fast optical probe with the Schlieren technique. We derive the required duration of the optical probe pulse ensuring discernibility of different singularities in the images. Although the internal nano-scale structure of the singularities remains unresolved, the important information about their location and mutual separation, including image rotation due to relativistic effects, can be accessed. For typical experimental parameters (multi-TW femtosecond lasers and underdense relativistic plasma), the separation d_0 can be as small as $\sim 5\,\mu$m. To discern multiple singularities, a few-μm optical resolution is necessary, which is achievable with existing imaging systems. The duration of the optical probe, τ_p, must be short enough to make the motion blur smaller than the separation between singularities: $c\tau_p < d_0$, which requires a few-cycle optical probe with sub-10 fs duration and corresponding motion blur $<3\,\mu$m. Such optical probes are already available,[31] which makes our scheme feasible with the modern laser facilities.

ACKNOWLEDGMENTS

The authors thank Dr. A. Bierwage for fruitful discussion. This work was supported by QST Director Fund 20, QST IRI, JSPS KAKENHI (No. JP19H00669), Ministry of Education, and Youth and Sports of the Czech Republic and European Regional Development Fund (No. CZ.02.1.01/0.0/0.0/15_003/0000449).

DATA AVAILABILITY

The data that support the findings of this study are available from the corresponding author upon reasonable request.

REFERENCES

[1]V. I. Arnold, *Catastrophe Theory*, 3rd ed. (Springer-Verlag Berlin Heidelberg, New York, 1992).
[2]T. Poston and I. Stewart, *Catastrophe Theory and Its Applications* (Dover Publications, Mineola, NY, USA, 1996).
[3]S. V. Bulanov, F. Pegoraro, A. M. Pukhov, and A. S. Sakharov, "Transverse-wake wave breaking," Phys. Rev. Lett. **78**, 4205–4208 (1997).
[4]T. Z. Esirkepov, Y. Kato, and S. V. Bulanov, "Bow wave from ultraintense electromagnetic pulses in plasmas," Phys. Rev. Lett. **101**, 265001–265004 (2008).
[5]A. S. Pirozhkov, M. Kando, T. Z. Esirkepov, P. Gallegos, H. Ahmed, E. N. Ragozin, A. Y. Faenov, T. A. Pikuz, T. Kawachi, A. Sagisaka, J. K. Koga, M. Coury, J. Green, P. Foster, C. Brenner, B. Dromey, D. R. Symes, M. Mori, K. Kawase, T. Kameshima, Y. Fukuda, L. Chen, I. Daito, K. Ogura, Y. Hayashi, H. Kotaki, H. Kiriyama, H. Okada, N. Nishimori, T. Imazono, K. Kondo, T. Kimura, T. Tajima, H. Daido, P. Rajeev, P. McKenna, M. Borghesi, D. Neely, Y. Kato, and S. V. Bulanov, "Soft-x-ray harmonic comb from relativistic electron spikes," Phys. Rev. Lett. **108**, 135004–135005 (2012).
[6]A. Zhidkov, J. Koga, K. Kinoshita, and M. Uesaka, "Effect of self-injection on ultraintense laser wake-field acceleration," Phys. Rev. E **69**, 035401(R) (2004).
[7]S. V. Bulanov, I. N. Inovenkov, V. I. Kirsanov, N. M. Naumova, and A. S. Sakharov, "Electromagnetic radiation frequency upshift upon interaction with nonlinear plasma waves," Sov. Phys.-Lebedev Inst. Rep. **6**, 9–11 (1991).
[8]S. V. Bulanov, T. Z. Esirkepov, and T. Tajima, "Light intensification towards the Schwinger limit," Phys. Rev. Lett. **91**, 085001 (2003).
[9]S. V. Bulanov, T. Z. Esirkepov, M. Kando, A. S. Pirozhkov, and N. N. Rosanov, "Relativistic mirrors in plasmas. Novel results and perspectives," Phys.-Usp. **56**, 429–464 (2013).
[10]M. Kando, T. Z. Esirkepov, J. Koga, A. S. Pirozhkov, and S. V. Bulanov, "Coherent, short-pulse x-ray generation via relativistic flying mirrors," Quantum Beam Sci. **2**, 9 (2018).
[11]M. Kando, Y. Fukuda, A. S. Pirozhkov, J. Ma, I. Daito, L. M. Chen, T. Z. Esirkepov, K. Ogura, T. Homma, Y. Hayashi, H. Kotaki, A. Sagisaka, M. Mori, J. K. Koga, H. Daido, S. V. Bulanov, T. Kimura, Y. Kato, and T. Tajima, "Demonstration of laser-frequency upshift by electron-density modulations in a plasma wakefield," Phys. Rev. Lett. **99**, 135001–135004 (2007).
[12]A. S. Pirozhkov, J. Ma, M. Kando, T. Z. Esirkepov, Y. Fukuda, L. M. Chen, I. Daito, K. Ogura, T. Homma, Y. Hayashi, H. Kotaki, A. Sagisaka, M. Mori, J. K. Koga, T. Kawachi, H. Daido, S. V. Bulanov, T. Kimura, Y. Kato, and T. Tajima, "Frequency multiplication of light back-reflected from a relativistic wake wave," Phys. Plasmas **14**, 123106–123122 (2007).
[13]A. S. Pirozhkov, T. Z. Esirkepov, M. Kando, Y. Fukuda, J. Ma, L. M. Chen, I. Daito, K. Ogura, T. Homma, Y. Hayashi, H. Kotaki, A. Sagisaka, M. Mori, J. K. Koga, T. Kawachi, H. Daido, S. V. Bulanov, T. Kimura, Y. Kato, and T. Tajima, "Demonstration of light reflection from the relativistic mirror," in Proceedings of IFSA 2007, Kobe, Japan, 9–14 September 2007, edited by H. Azechi, B. Hammel, and J.-C. Gauthier, 2007 [J. Phys.: Conf. Ser. **112**, 042050–042054 (2008)].
[14]A. S. Pirozhkov, M. Kando, T. Z. Esirkepov, J. Ma, Y. Fukuda, L. M. Chen, I. Daito, K. Ogura, T. Homma, Y. Hayashi, H. Kotaki, A. Sagisaka, M. Mori, J. K. Koga, T. Kawachi, H. Daido, S. V. Bulanov, T. Kimura, Y. Kato, and T. Tajima, "Relativistic tennis using flying mirror," in Proceedings of the Laser-Driven Relativistic Plasmas Applied for Science, Industry, and Medicine: The 1st International Symposium, Kyoto (Japan), 17–20 September 2007, edited by P. R. Bolton, H. Daido, and S. V. Bulanov, 2017 [AIP Conf. Proc. **1024**, 37–51 (2008)].
[15]M. Kando, A. S. Pirozhkov, K. Kawase, T. Z. Esirkepov, Y. Fukuda, H. Kiriyama, H. Okada, I. Daito, T. Kameshima, Y. Hayashi, H. Kotaki, M. Mori, J. K. Koga, H. Daido, A. Y. Faenov, T. Pikuz, J. Ma, L. M. Chen, E. N. Ragozin, T. Kawachi, Y. Kato, T. Tajima, and S. V. Bulanov, "Enhancement of photon number reflected by the relativistic flying mirror," Phys. Rev. Lett. **103**, 235003–235004 (2009).
[16]A. S. Pirozhkov, M. Kando, T. Z. Esirkepov, Y. Fukuda, L.-M. Chen, I. Daito, K. Ogura, T. Homma, Y. Hayashi, H. Kotaki, A. Sagisaka, M. Mori, J. K. Koga, T. Kawachi, H. Kiriyama, H. Okada, K. Kawase, T. Kameshima, N. Nishimori, E. N. Ragozin, A. Y. Faenov, T. A. Pikuz, T. Kimura, T. Tajima, H. Daido, Y. Kato, and S. V. Bulanov, "Demonstration of flying mirror with improved efficiency," in Proceedings of the 2nd International Symposium on Laser-Driven Relativistic Plasmas Applied to Science, Industry and Medicine, Kyoto (Japan), 19–23 January 2009, edited by P. R. Bolton, H. Daido, and S. V. Bulanov, 2009 [AIP Conf. Proc. **1153**, 274–284 (2009)].
[17]M. Kando, A. S. Pirozhkov, Y. Fukuda, T. Z. Esirkepov, I. Daito, K. Kawase, J. L. Ma, L. M. Chen, Y. Hayashi, M. Mori, K. Ogura, H. Kotaki, A. Sagisaka, E. N. Ragozin, A. Faenov, T. Pikuz, H. Kiriyama, H. Okada, T. Kameshima, J. K. Koga, K. Belyaev, F. F. Kamenets, A. Sugiyama, T. Kawachi, H. Daido, T. Kimura, Y. Kato, T. Tajima, and S. V. Bulanov, "Experimental studies of the high and low frequency electromagnetic radiation produced from nonlinear laser-plasma interactions," Eur. Phys. J. D **55**, 465–474 (2009).
[18]A. S. Pirozhkov, M. Kando, T. Z. Esirkepov, P. Gallegos, H. Ahmed, E. N. Ragozin, A. Y. Faenov, T. A. Pikuz, J. K. Koga, H. Kiriyama, P. McKenna, M. Borghesi, K. Kondo, H. Daido, Y. Kato, D. Neely, and S. V. Bulanov, "Coherent x-ray generation in relativistic laser/gas jet interactions," in Proceedings of the X-Ray Lasers and Coherent X-Ray Sources: Development and Applications IX, San Diego, California, USA 23–25 August 2011, edited by J. Dunn and A. Klisnick, 2011 [Proc. SPIE **8140**, 81400A–81416A (2011)].
[19]G. A. Askaryan, "Effect of the gradient of a strong electromagnetic ray on electrons and atoms," Zh. Eksp. Teor. Fiz. **42**, 1567–1570 (1962).
[20]A. Litvak, "Finite-amplitude wave beams in a magnetoactive plasma," Sov. Phys. JETP **30**, 344 (1970).
[21]G. Z. Sun, E. Ott, Y. C. Lee, and P. Guzdar, "Self-focusing of short intense pulses in plasmas," Phys. Fluids **30**, 526–532 (1987).
[22]S. S. Bulanov, V. Y. Bychenkov, V. Chvykov, G. Kalinchenko, D. W. Litzenberg, T. Matsuoka, A. G. R. Thomas, L. Willingale, V. Yanovsky, K. Krushelnick, and A. Maksimchuk, "Generation of GeV protons from 1 PW

© Author(s) 2020

laser interaction with near critical density targets," Phys. Plasmas **17**, 043105–043108 (2010).
[23]T. Pikuz, A. Faenov, A. Pirozhkov, A. Astapov, G. Klushin, S. Pikuz, N. Nagorskiy, S. Magnitskiy, T. Esirkepov, J. Koga, T. Nakamura, S. Bulanov, Y. Fukuda, Y. Hayashi, H. Kotaki, Y. Kato, and M. Kando, "High performance imaging of relativistic soft X-ray harmonics by sub-micron resolution LiF film detectors," Phys. Status Solidi C **9**, 2331–2335 (2012).
[24]A. S. Pirozhkov, M. Kando, T. Z. Esirkepov, P. Gallegos, H. Ahmed, E. N. Ragozin, A. Y. Faenov, T. A. Pikuz, T. Kawachi, A. Sagisaka, J. K. Koga, M. Coury, J. Green, P. Foster, C. Brenner, B. Dromey, D. R. Symes, M. Mori, K. Kawase, T. Kameshima, Y. Fukuda, L. Chen, I. Daito, K. Ogura, Y. Hayashi, H. Kotaki, H. Kiriyama, H. Okada, N. Nishimori, T. Imazono, K. Kondo, T. Kimura, T. Tajima, H. Daido, P. Rajeev, P. McKenna, M. Borghesi, D. Neely, Y. Kato, and S. V. Bulanov, "High order harmonics from relativistic electron spikes," New J. Phys. **16**, 093003–093030 (2014).
[25]A. S. Pirozhkov, M. Kando, T. Z. Esirkepov, P. Gallegos, H. Ahmed, E. N. Ragozin, A. Y. Faenov, T. A. Pikuz, T. Kawachi, A. Sagisaka, J. K. Koga, M. Coury, J. Green, P. Foster, C. Brenner, B. Dromey, D. R. Symes, M. Mori, K. Kawase, T. Kameshima, Y. Fukuda, L. M. Chen, I. Daito, K. Ogura, Y. Hayashi, H. Kotaki, H. Kiriyama, H. Okada, N. Nishimori, T. Imazono, K. Kondo, T. Kimura, T. Tajima, H. Daido, P. Rajeev, P. McKenna, M. Borghesi, D. Neely, Y. Kato, and S. V. Bulanov, "Relativistic high harmonic generation in gas jet targets" in Proceedings of the 3rd International Symposium on Laser-Driven Relativistic Plasmas Applied to Science, Energy, Industry, and Medicine, Kyoto, Japan, 30 May–2 June 2011, edited by S. V. Bulanov, A. Yokoyama, Y. I. Malakhov, and Y. Watanabe, 2011 [AIP Conf. Proc. **1465**, 167–171 (2012)].
[26]A. S. Pirozhkov, T. Z. Esirkepov, T. A. Pikuz, A. Y. Faenov, K. Ogura, Y. Hayashi, H. Kotaki, E. N. Ragozin, D. Neely, H. Kiriyama, J. K. Koga, Y. Fukuda, A. Sagisaka, M. Nishikino, T. Imazono, N. Hasegawa, T. Kawachi, H. Daido, Y. Kato, S. V. Bulanov, K. Kondo, and M. Kando, "High-order harmonic generation by relativistic plasma singularities: The driving laser requirements," in Proceedings of X-Ray Lasers 2016, Nara, Japan, 22–27 May 2016, edited by T. Kawachi, S. V. Bulanov, H. Daido, and Y. Kato, 2016 [Springer Proc. Phys. **202**, 85–92 (2018)].
[27]A. S. Pirozhkov, T. Z. Esirkepov, T. A. Pikuz, A. Y. Faenov, A. Sagisaka, K. Ogura, Y. Hayashi, H. Kotaki, E. N. Ragozin, D. Neely, J. K. Koga, Y. Fukuda, M. Nishikino, T. Imazono, N. Hasegawa, T. Kawachi, H. Daido, Y. Kato, S. V. Bulanov, K. Kondo, H. Kiriyama, and M. Kando, "Laser requirements for high-order harmonic generation by relativistic plasma singularities," Quantum Beam Sci. **2**, 7 (2018).
[28]A. S. Pirozhkov, T. Z. Esirkepov, T. A. Pikuz, A. Y. Faenov, K. Ogura, Y. Hayashi, H. Kotaki, E. N. Ragozin, D. Neely, H. Kiriyama, J. K. Koga, Y. Fukuda, A. Sagisaka, M. Nishikino, T. Imazono, N. Hasegawa, T. Kawachi, P. R. Bolton, H. Daido, Y. Kato, K. Kondo, S. V. Bulanov, and M. Kando, "Burst intensification by singularity emitting radiation in multi-stream flows," Sci. Rep. **7**, 17968 (2017).
[29]M. C. Downer, R. Zgadzaj, A. Debus, U. Schramm, and M. C. Kaluza, "Diagnostics for plasma-based electron accelerators," Rev. Mod. Phys. **90**, 035002 (2018).
[30]N. H. Matlis, S. Reed, S. S. Bulanov, V. Chvykov, G. Kalintchenko, T. Matsuoka, P. Rousseau, V. Yanovsky, A. Maksimchuk, S. Kalmykov, G. Shvets, and M. C. Downer, "Snapshots of laser wakefields," Nat. Phys. **2**, 749–753 (2006).
[31]A. Sävert, S. P. D. Mangles, M. Schnell, E. Siminos, J. M. Cole, M. Leier, M. Reuter, M. B. Schwab, M. Möller, K. Poder, O. Jäckel, G. G. Paulus, C. Spielmann, S. Skupin, Z. Najmudin, and M. C. Kaluza, "Direct observation of the injection dynamics of a laser wakefield accelerator using few-femtosecond shadowgraphy," Phys. Rev. Lett. **115**, 055002 (2015).
[32]E. Siminos, S. Skupin, A. Sävert, J. M. Cole, S. P. D. Mangles, and M. C. Kaluza, "Modeling ultrafast shadowgraphy in laser-plasma interaction experiments," Plasma Phys. Controlled Fusion **58**, 065004 (2016).
[33]M. B. Schwab, E. Siminos, T. Heinemann, D. Ullmann, F. Karbstein, S. Kuschel, A. Sävert, M. Yeung, D. Hollatz, A. Seidel, J. Cole, S. P. D. Mangles, B. Hidding, M. Zepf, S. Skupin, and M. C. Kaluza, "Visualization of relativistic laser pulses in underdense plasma," Phys. Rev. Accel. Beams **23**, 032801 (2020).
[34]U. Kraus, "Brightness and color of rapidly moving objects: The visual appearance of a large sphere revisited," Am. J. Phys. **68**(1), 56 (2000).
[35]T. Z. Esirkepov, "Exact charge conservation scheme for particle-in-cell simulation with an arbitrary form-factor," Comput. Phys. Commun. **135**, 144–153 (2001).
[36]J. Mu, T. Zh. Esirkepov, Y. Gu, T. M. Jeong, P. Valenta, A. S. Pirozhkov, J. K. Koga, M. Kando, G. Korn, and S. V. Bulanov, "Boosted high order harmonics from electron density singularity formed at the relativistic laser bow wave," arXiv:1904.05574 (2019).
[37]T. Esirkepov, S. V. Bulanov, M. Yamagiwa, and T. Tajima, "Electron, positron, and photon wakefield acceleration: Trapping, wake overtaking, and ponderomotive acceleration," Phys. Rev. Lett. **96**, 014803 (2006).
[38]A. G. R. Thomas, S. P. D. Mangles, Z. Najmudin, M. C. Kaluza, C. D. Murphy, and K. Krushelnick, "Measurements of wave-breaking radiation from a laser-wakefield accelerator," Phys. Rev. Lett. **98**, 054802 (2007).
[39]A. Rousse, K. T. Phuoc, R. Shah, A. Pukhov, E. Lefebvre, V. Malka, S. Kiselev, F. Burgy, J.-P. Rousseau, D. Umstadter, and D. Hulin, "Production of a keV x-ray beam from synchrotron radiation in relativistic laser-plasma interaction," Phys. Rev. Lett. **93**, 135005 (2004).
[40]S. Kneip, C. McGuffey, J. L. Martins, S. F. Martins, C. Bellei, V. Chvykov, F. Dollar, R. Fonseca, C. Huntington, G. Kalintchenko, A. Maksimchuk, S. P. D. Mangles, T. Matsuoka, S. R. Nagel, C. A. J. Palmer, J. Schreiber, K. T. Phuoc, A. G. R. Thomas, V. Yanovsky, L. O. Silva, K. Krushelnick, and Z. Najmudin, "Bright spatially coherent synchrotron X-rays from a table-top source," Nat. Phys. **6**, 980–983 (2010).
[41]K. Huang, Y. F. Li, D. Z. Li, L. M. Chen, M. Z. Tao, Y. Ma, J. R. Zhao, M. H. Li, M. Chen, M. Mirzaie, N. Hafz, T. Sokollik, Z. M. Sheng, and J. Zhang, "Resonantly enhanced betatron hard X-rays from ionization injected electrons in a laser plasma accelerator," Sci. Rep. **6**, 27633 (2016).
[42]F. Albert, N. Lemos, J. L. Shaw, B. B. Pollock, C. Goyon, W. Schumaker, A. M. Saunders, K. A. Marsh, A. Pak, J. E. Ralph, J. L. Martins, L. D. Amorim, R. W. Falcone, S. H. Glenzer, J. D. Moody, and C. Joshi, "Observation of betatron x-ray radiation in a self-modulated laser wakefield accelerator driven with picosecond laser pulses," Phys. Rev. Lett. **118**, 134801 (2017).

© Author(s) 2020